Combustion Theory and Modelling, 2018
https://doi.org/10.1080/13647830.2018.1465206

Taylor & Francis
Taylor & Francis Group

Check for updates

Effect of local variations of the laminar flame speed on the global finger-flame acceleration scenario

Sinan Demir, Hayri Sezer and V'yacheslav Akkerman*

Center for Innovation in Gas Research and Utilization (CIGRU), Center for Alternative Fuels, Engines and Emissions (CAFEE), Computational Fluid Dynamics and Applied Multi-Physics Center, Department of Mechanical and Aerospace Engineering, West Virginia University, Morgantown, WV 26506-6106, USA

(*Received 26 July 2017; accepted 3 April 2018*)

Numerous formulations describing the dynamics and morphology of corrugated flames, including the scenarios of flame acceleration, are based on a "geometrical consideration", where the wrinkled-to-planar flame velocities ratio, S_w/S_L, is evaluated as the scaled flame surface area, while the entire combustion chemistry is immersed into the planar flame speed S_L, which is assumed to be constant. However, S_L may experience noticeable spatial/temporal variations in practice, in particular, due to pressure/temperature variations as well as non-uniform distribution of the equivalence ratio and/or that of combustible or inert dust impurities. The present work initiates the systematic study of the impact of the local S_L-variations on the global flame evolution scenario. The variations are assumed to be imposed externally, in a manner being a free functional of the formulation. Specifically, the linear, parabolic and hyperbolic spatial S_L-distributions are incorporated into the formulations of finger flame acceleration in pipes, and they are compared to the case of constant S_L. Both two-dimensional channels and cylindrical tubes are considered. The conditions promoting or moderating flame acceleration are identified, and the revisited equations for the flame shape, velocity and acceleration rate are obtained for various S_L-distributions. The theoretical findings are validated by the computational simulations of the reacting flow equations, with agreement between the theory and modelling demonstrated.

Keywords: Premixed flames; unstretched laminar burning velocity; corrugated flame velocity; finger flames; flame acceleration; computational simulations

1. Introduction

The unstretched laminar burning velocity S_L – a speed with which a planar premixed flame front propagates with respect to the unburnt mixture – constitutes one of the key parameters characterising premixed combustion, and it is investigated reasonably well for the majority of fuels [1]. However, such a planar flame occurs ultimately seldom in practice; industrial and laboratory flames are usually corrugated. Various factors can contribute to flame corrugation, including combustion instabilities, acoustic–flame interactions, turbulence and the characteristics of combustor geometry such as smooth or obstructed walls, aspect ratios, etc. [2]. A corrugated flame front has a larger surface area relative to a planar flame, involving the same mixture and under the same conditions; therefore, such a corrugated flame consumes more fuel and release more heat per unit time, thereby propagating faster

*Corresponding author. Email: Vyacheslav.Akkerman@mail.wvu.edu

© 2018 Informa UK Limited, trading as Taylor & Francis Group

than the planar one. Thus, continuous increase in the flame surface area provides continuous flame acceleration [3].

Numerous theories, associated with the variety of flame acceleration scenarios, are based on the so-called "geometrical formulation": namely, the wrinkled-to-planar flame speeds ratio, S_w/S_L, is evaluated as the respective corrugated flame surface area, scaled by the planar one, while the entire combustion chemistry is immersed into S_L. The latter has conventionally been considered as a constant depending on the thermal-chemical properties of the fuel mixture only, irrespective of a configuration and hydrodynamics [4–6]. However, in practice, the value of S_L may experience spatial and temporal variations, caused by heat losses [7] or non-uniform distribution of the equivalence ratio [8], as well as due to the associated pressure and temperature variations [9,10] or, as in coalmines, due to the local variations of the coal dust and/or rock dust impurities [11,12].

In fact, variations of the planar flame speed have been addressed in a number of studies. In particular, Grune et al. [13,14] analysed, experimentally, deflagration-to-detonation transitions in stratified hydrogen–air mixtures in semi-confined geometry with various linear gradients of the hydrogen concentration. Shi et al. [15] showed the effect of stratification on the laminar burning velocity by means of a numerical analysis of the local fuel consumption, burnt gas expansion, as well as the hydrodynamic effects of the flow velocity variations. Hemchandra and Lieuwen [16] demonstrated a significant role of the local spatial variations of the consumption flame velocity, along the flame front, in the presence of turbulence. However, none of these works provided a guidance on how to combine local and global flame dynamics, while the controlling strategies of how to prevent or promote flame acceleration need rigorous quantitative assessment of the impacts of local S_L- variations on the global flame front morphology and on its propagation velocity S_w.

To address this demand, we initiate a systematic study of how to incorporate the local variations of the planar flame velocity into formulations on the global, corrugated flame velocity in the cases when the S_L-distribution is imposed externally, being an arbitrary function employed in the formulation. The present work is the first step in this direction. Specifically, here we focus on the mechanism of flame acceleration associated with a finger-like shape of the flame front at the initial stages of burning in pipes; the impact of S_L-variations on other acceleration mechanisms, such as the Shelkin mechanism of acceleration due to friction at the wall roughness [3] and/or acceleration due to in-built obstacles [17], will be scrutinised elsewhere. Such a finger-flame acceleration mechanism was identified, first, in the experiments by Clanet and Searby [18] and subsequently investigated, by means of theory and modelling, by Bychkov et al. [5,19]. Recently, Demir et al. [20,21] extended the finger flame formulations to consider accidental methane–air–dust fires in coalmines. In that case, the hydrodynamic flame instability plays a noticeable role in the acceleration process, because of the large scales involved in the problem.

The general scenario of finger flame acceleration is as follows. A flame front propagating from the closed end of a semi-open pipe evolves from an initially hemispherical shape to a finger shape. The flame surface area grows exponentially in time, such that the growth rate is high, but this occurs only during a short time interval [5], namely, acceleration lasts until a flame "skirt" contacts a pipe sidewall. In the present work, we revisit the finger flame formulation [5] to account for the local variations of the laminar burning velocity S_L. Starting with $S_L = const$, we then incorporate the linear, parabolic and hyperbolic spatial S_L-distributions into the analysis. In this respect, we thereby develop the theory of flame acceleration due to a finger-like flame shape for the two-dimensional (2D) planar and cylindrical axisymmetric geometries, accounting for S_L-variations. The theoretical findings are subsequently validated by means of the computational simulations of the reacting flow

equations, with fully compressible hydrodynamics, transport properties and Arrhenius chemical kinetics.

2. Formulation

While an analysis of S_L-distributions occurring in practice would require further detail, we start with the simplest distributions allowing an analytical consideration, and compare them to the situation of $S_L = S_{L,0} = const$. Specifically, linear, parabolic and hyperbolic S_L-distributions in the 2D planar and cylindrical axisymmetric geometries are employed:

$$S_L = S_{L,0}\left(a - \varsigma\left|\frac{r}{R}\right|\right), \quad S_L = S_{L,0}\left(a - \varsigma\left(\frac{r}{R}\right)^2\right),$$
$$S_L = S_{L,0}\frac{\tanh\left\{a\left(a - \varsigma(r/R)^2\right)\right\}}{\tanh a}, \tag{1}$$

where $S_{L,0}$ would be the referenced planar flame speed in the case of uniform S_L-distribution, while a and ς are the free parameters of the formulation. In our study, the local flame velocity at the sidewall always exceeds zero as otherwise a flame skirt would never contact the sidewall, which would yield unlimited flame acceleration. In particular, here we employ $a = 1$ and $\varsigma = 0.8$ to provide strong acceleration nearby the tube centreline but weak acceleration near the wall, thereby moderating global flame acceleration. In contrast, to promote flame spreading at the sidewall while moderating it at the centreline, we took $a = 0.2$, $\varsigma = -0.8$. The distributions of Equation (1) are presented in Figure 1. While the linear distribution is the most encountered one in many studies [13,14,22], the distributions of Equation (1) are considered in this work for the following reasons: first, being simple from the analytical viewpoint, these distributions can actually be of practical relevance. In fact, the coal-dust distribution is typically non-uniform in coalmines, where a stationary dense coal-dust layer may spread through the bottom of a passage. In particular, a gaseous-based detonation wave may produce a strong shock that can lift and entrain the dust layer. Over time, this shock wave weakens, but the fluid, heated by the shock wave, is ignited by the lifted dust, which initiates a secondary combustion process [22]. Such a lifted dust layer may resemble a linear, cubic, or even parabolic distribution of the dust concentration in space, due to the different energy levels of complex magnetic forces. The impact of these local

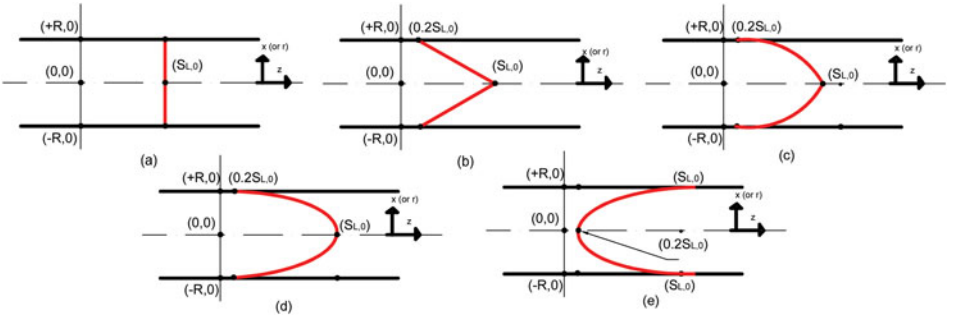

Figure 1. Schematic of various S_L-distributions, Equation (1): (a) constant, (b) linear, (c) tangential-hyperbolic, (d) parabolic (promotion along the axis, $a = 1, \varsigma = 0.8$), and Equation (13): (e) parabolic (promotion through the wall, $a = 0.2$, $\varsigma = -0.8$).

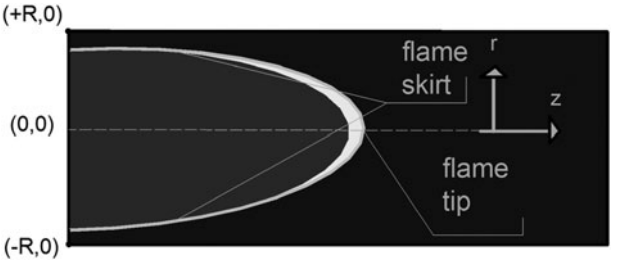

Figure 2. Schematic of the finger-flame acceleration mechanism.

spatial variations of the burning properties on global flame propagation will be presented in the following sections. Second, the planar flame speed depends on the major thermal parameters (such as the Lewis number, Le, thermal conductivity, λ, fuel concentration, χ, density, ρ, burnt gas temperature T_b, etc.) as $S_L \propto \sqrt{f(Le, \rho, \lambda, \chi)\exp(-E_a/RT_b)}$. Therefore, any linear variation of Le, ρ, λ, or χ (under square root) corresponds to a hyperbolic-like S_L-function. Similarly, any local temperature variations in the exponential term can generate a parabolic-like variation of the laminar flame velocity. This situation may also justify the physical interpretation of our distribution functions. It should be noted that these distributions do not have the same averaged flame velocity along the cross section since the current aim of this study is to analyse the effect of different distributions.

We consider a flame propagating in a 2D planar channel or an axisymmetric cylindrical tube of radius (half-width) R, with slip adiabatic walls and with one end closed, as illustrated in Figure 2. The ignition point is at the closed end at the symmetry axis (centreline). The mechanism of "finger flame" acceleration is the following: when a flame front starts approaching the channel/tube wall, it acquires a finger-like shape due to the difference between the radial and axial velocities [5]. Then the flame surface area grows quite fast, increasing the flame velocity by an order of magnitude by the time when the flame skirt contacts the sidewall. Thereafter, such finger-shape-based acceleration stops, followed by a convex-to-concave conversion of the flame shape and formation of a "tulip flame" [5,18]. Nevertheless, the present work is limited to the finger-shaped stage of the flame evolution. Within the theoretical formulation of [5], the nature of finger flame acceleration is Reynolds-independent such that acceleration is equally strong in mining passages and micro-pipes. However, in practice, Reynolds-dependent factors such as combustion instabilities and/or turbulence will provide the corrections to the flame acceleration scenario. One may potentially include the effect of turbulence into an analysis by replacing the planar flame velocity S_L with a local wrinkled/turbulent burning velocity S_w [20]. As of now, we next incorporate the S_L-dependences (1) into a theory of finger flame acceleration for the 2D planar and cylindrical axisymmetric cases. Similar to [5,19], the unity Lewis number is employed throughout the analyses to avoid the diffusional-thermal instability.

2.1. *Two-dimensional (2D) planar geometry*

To develop a 2D finger flame formulation, we start with the incompressible continuity equation:

$$\frac{\partial u_x}{\partial x} + \frac{\partial u_z}{\partial z} = 0, \tag{2}$$

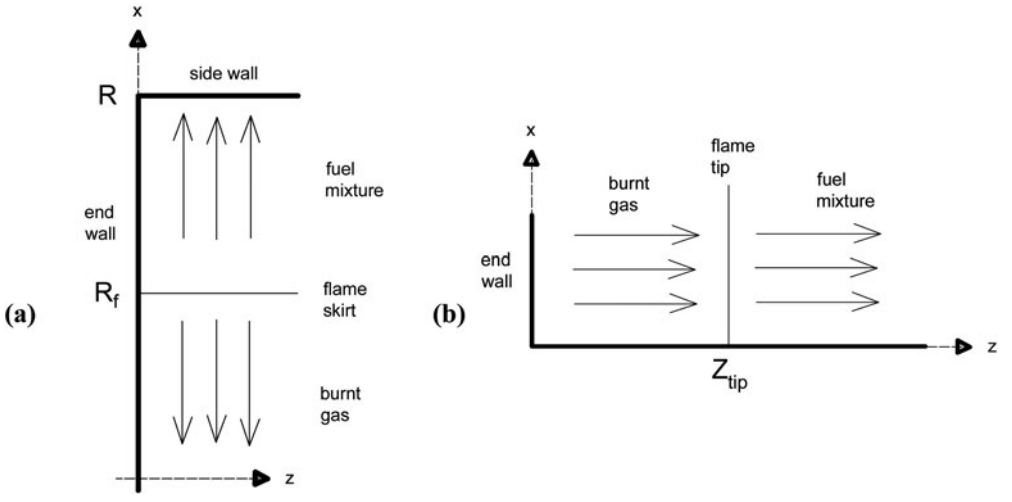

Figure 3. A flow close to the pipe end-wall (a) and the centreline (b).

with the boundary conditions $u_z|_{z=0} = 0$, $u_x|_{x=X_f} = 0$, where $X_f(t)$ denotes the flame "skirt". A conventional (Landau) approach of an infinitesimally thin flame front is adopted. Figure 3 describes the coordinate system for the flow near the end-wall (Figure 3(a)) and the centreline (Figure 3(b)) of the channel. Assuming a potential flow in the fuel mixture (label "1"), we find the flow velocity components from the equation of continuity, Equation (2) as:

$$u_{z,1} = A_1 z, \qquad u_{x,1} = A_1 (R - x), \tag{3}$$

where the factor A_1 may depend on time, $A_1(t)$, and it will be discussed below. The counterpart of Equation (3) in the burnt matter (label "2") reads:

$$u_{z,2} = A_2 z, \qquad u_{x,2} = -A_2 x, \tag{4}$$

with a certain factor $A_2(t)$. It is noted that while the flow is generally rotational in the burnt matter (with singularity occurring), due to a curved flame shape, this flow can be treated as a potential flow close to the end-wall, where the flame front is locally planar. Hence, the baroclinic effects due to the local perturbation can be neglected in that region. The matching conditions at the flame front are:

$$\frac{dX_f}{dt} - u_{x,1} = S_L\left(X_f\right), \quad u_{x,1} - u_{x,2} = (\Theta - 1)\, S_L\left(X_f\right), \quad u_{z,1} = u_{z,2}, \tag{5}$$

where $\Theta \equiv \rho_{fuel}/\rho_{burnt}$ is the thermal expansion ratio (the density drop on the flame front). In Equation (5), the first relation specifies a locally variable flame propagation speed with respect to the fuel mixture, the second condition describes the jump of the normal velocity component, and the third relation shows the continuity of the tangential velocity component. Together, Equations (3)–(5) yield $A_1(t) = A_2(t) = (\Theta - 1)S_L[X_f(t)]/R$ such that the final

evolution equation for the flame skirt position reads:

$$\frac{dX_f}{dt} = S_L\left(X_f\right)\left[\Theta - (\Theta - 1)\frac{X_f}{R}\right]. \tag{6}$$

Similarly, we can also find the evolution equation for the flame tip position, Z_{tip}, by considering the flow along the channel centreline $x = 0$, similar to Equation (6), and with Equation (4) for $u_{z,2,}$, namely:

$$\frac{dZ_{tip}}{dt} - u_{z,2} = \frac{dZ_{tip}}{dt} - (\Theta - 1)\, S_L\left(X_f(t)\right)\frac{Z_{tip}}{R} = \Theta\, S_{L,0}. \tag{7}$$

In fact, Equation (7) describes propagation of the flame tip with respect to the burnt matter. It is noted that this equation works as long as the flame tip is at the centreline, such that the flame front is locally planar therein and the flow in the burnt matter can be treated as potential. However, this is not the case if the tip is far from the centreline, because the flow is rotational in that event.

2.2. *Cylindrical, axisymmetric geometry*

Here we reproduce the 2D formulation above for the cylindrical axisymmetric geometry. Then the continuity equation for the incompressible flow reads [5]:

$$\frac{1}{r}\frac{\partial(u_r r)}{\partial r} + \frac{\partial u_z}{\partial z} = 0, \tag{8}$$

with the boundary conditions $u_z|_{z=0} = 0$, $u_r|_{r=R_f} = 0$, where $R_f(t)$ describes the flame skirt in the cylindrical geometry. Similar to the 2D case, assuming potential flow in the fuel mixture, we find the axial and radial flow velocity components from Equation (8) as:

$$u_{z,1} = A_1 z, \quad u_{r,1} = \frac{A_1}{2}\left(\frac{R^2}{r} - r\right), \tag{9}$$

with a certain time-dependent factor $A_1(t)$. The counterpart of Equation (9) in the burnt matter reads:

$$u_{z,2} = A_2 z, \quad u_{r,2} = -\frac{A_2}{2} r, \tag{10}$$

where $A_2 = A_2(t)$. The matching conditions are the same as those in the 2D planar geometry, i.e. Equation (5). Then $A_1 = A_2 = (\Theta - 1)S_L[R_f(t)] \cdot R_f(t)/R$ such that the evolution equation for flame skirt reads:

$$\frac{dR_f}{dt} = S_L\left(R_f\right)\left[\Theta - (\Theta - 1)\left(\frac{R_f}{R}\right)^2\right]. \tag{11}$$

We can also derive the evolution equation for the flame tip in the cylindrical geometry, similar to the 2D case, by considering the flow along the centreline, $r = 0$, where the flame

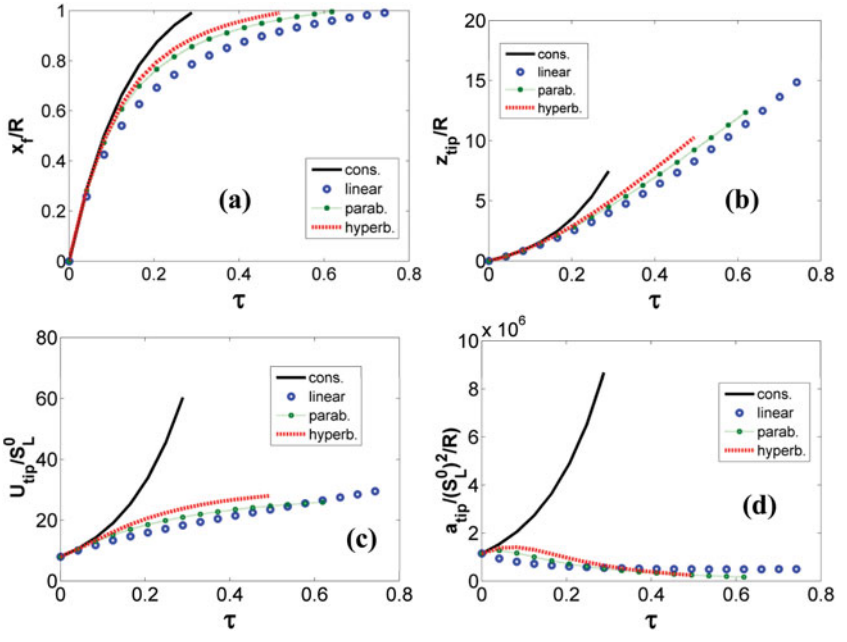

Figure 4. 2D planar geometry: evolution of the scaled flame skirt position (a), flame tip position (b), flame tip velocity (c), and flame tip acceleration (d) for a constant, linear, hyperbolic and parabolic S_L-distributions.

front is locally planar and the flow in the burnt matter is potential, such that:

$$\frac{dZ_{tip}}{dt} - 2\left(\Theta - 1\right) S_L\left(R_f(t)\right) \frac{R_f(t) Z_{tip}}{R^2} = \Theta\, S_{L,0}. \tag{12}$$

3. Results

We first incorporate various spatial dependences of the planar flame velocity into the final evolution equations for the flame skirt and tip, namely $S_L(X_f)$ into Equations (6) and (7) in a 2D planar geometry, and $S_L(R_f)$ into Equations (11) and (12) in a cylindrical axisymmetric configuration. In each geometry, the final set of equations is solved numerically by employing a fourth-order Runge–Kutta iterative method, with $\Theta = 8$, typical for hydrocarbon flames [1], employed in all cases.

Figure 4 presents the time evolution of the scaled flame skirt position, X_f/R (Figure 4(a)), and the scaled flame tip position, Z_{tip}/R (Figure 4(b)), as well as the scaled flame tip velocity, $U_{tip}/S_{L,0}$ (Figure 4(c)), and its scaled acceleration, $a_{tip}R/S_{L,0}^2$ (Figure 4(d)), in a 2D planar geometry, with various distributions of S_L being compared in each plot. Here $U_{tip} = dZ_{tip}/dt$, $a_{tip} = d^2Z_{tip}/dt^2$, and the scaled time is $\tau = tS_{L,0}/R$. According to Figure 4(a), the flame skirt reaches the wall in the promptest manner for $S_L = S_{L,0} = const$ as compared to other distributions; followed by the hyperbolic, parabolic and linear S_L-distributions, respectively. This is also true for the evolution of the flame tip velocity shown in Figure 4(c). The finger-flame acceleration mechanism stops when the flame skirt contacts a sidewall, $X_f/R = 1$. The maximum flame tip position at this time, among various distributions of S_L, is that for a linear distribution (simply because the process

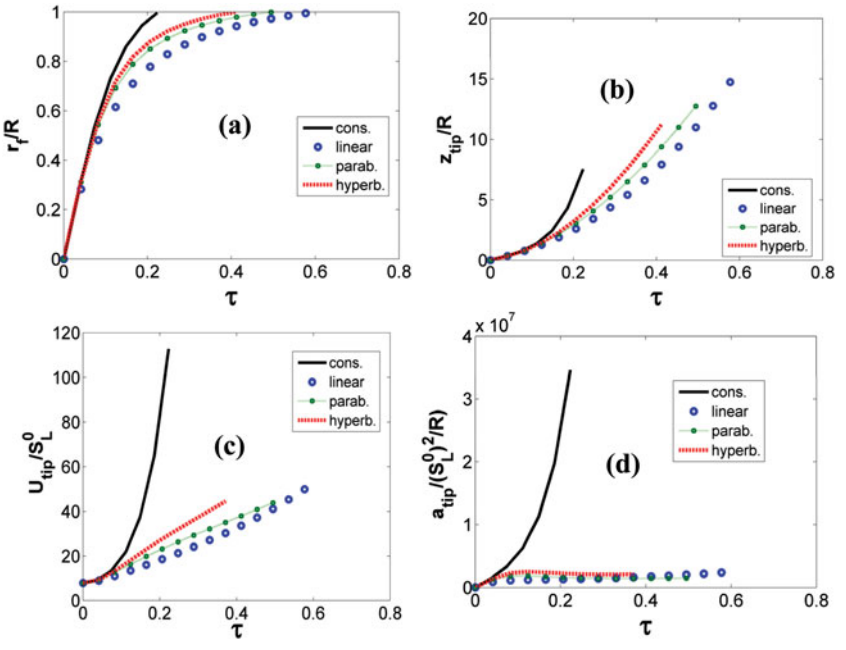

Figure 5. Cylindrical axisymmetric geometry: evolution of the flame skirt position (a), flame tip position (b), flame tip velocity (c), and flame tip acceleration (d) for constant, linear, hyperbolic and parabolic S_L-distributions.

takes the longest time in that case); followed by a parabolic, hyperbolic and constant S_L-distributions, respectively. The largest flame tip velocity in Figure 4(c) is observed for the linear case, followed by the hyperbolic and parabolic ones. Figure 4(d) shows the evidence of strong acceleration for all considered functions. Indeed, for a typical hydrocarbon flame this acceleration exceeds gravity acceleration by a factor of $\sim 10^3$! Figure 5 is a counterpart of Figure 4 for the cylindrical axisymmetric geometry. It is seen that the 2D planar and the cylindrical axisymmetric results agree qualitatively, but they differ quantitatively, providing larger quantities for the cylindrical case. According to Figure 5(a), the flame skirt contacts the sidewall in the promptest manner for the constant S_L, followed by the hyperbolic, parabolic and linear distributions. Again, flame acceleration stops when $R_f/R = 1$.

One of the key observations from Figures 4 and 5 is moderation of the acceleration regime for the non-uniform S_L-distributions as compared to the case of $S_L = S_{L,0} = const$. Indeed, while we observe exponential flame acceleration for a constant S_L in both 2D planar and cylindrical axisymmetric geometries, the acceleration trend moderates to a near-linear one for non-uniform S_L. It is also noted that the maximum flame tip velocity is observed in the cylindrical geometry for a constant S_L, and it is $\sim 115\, S_L$, which still obeys the approach of an incompressible flow for a typical hydrocarbon flame (indeed, the speed of sound to the laminar burning velocity ratio is $c_o/S_L \sim 10^3$ for such a flame). However, for highly reactive mixtures such as hydrogen–oxygen and/or ethylene–oxygen, the respective flame tip velocity would approach the speed of sound, such that applying compressible flow characteristics would be of key importance [19].

Overall, it is seen from Figures 4 and 5 that the evolutions of the flame shape, location and velocity differ for various functions describing the spatial S_L-distributions. Consequently, by manipulating and imposing these functions, one can potentially be able to control the flame

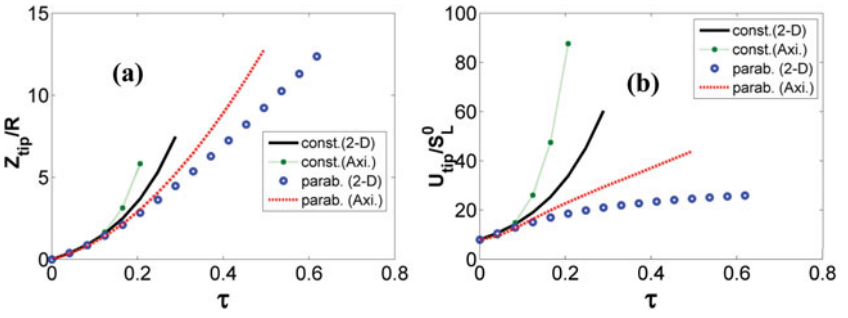

Figure 6. Comparison of the 2D planar and cylindrical axisymmetric cases for the constant and parabolic S_L-distributions: evolution of the scaled flame tip position (a) and velocity (b).

propagation mechanisms. It is noted again that, among the distributions of S_L considered in this work, the uniform distribution provides fastest flame acceleration followed by the hyperbolic distribution. The latter shows the largest elongation through the upper and lower segments of the flame front; see Figure 1(c). As a result, the flame surface area increases more than that for other non-uniform S_L-distributions, thereby enhancing flame propagation.

To understand better the effect of geometry, both 2D planar and cylindrical axisymmetric configurations are compared in Figure 6, with the scaled flame tip positions and velocities depicted in Figures 6(a) and 6(b), respectively. Here, the constant and parabolic S_L-distributions are employed in both cases. It is seen that a flame propagates/accelerates faster in a cylindrical configuration as compared to a 2D planar one with the same thermal-chemistry. For a parabolic S_L-distribution, the choice of geometry influences the scaled flame tip velocity significantly: it is almost twice larger for the cylindrical axisymmetric configuration than that in the 2D planar geometry.

In fact, various S_L-distributions with various selected free parameters a and ς can either promote or moderate the flame acceleration scenario as discussed earlier. All the distributions of Equation (1) moderate flame acceleration as compared to the case of $S_L = S_{L,0} = const$. Indeed, they provide stronger acceleration through the centreline, but weaker acceleration through the wall and, as a result, moderate the global flame dynamics. In fact, this is often the case in practice, for instance, in the pipe-like combustors, which experience wall heat losses and, thereby, provide slower flame spreading along the wall, but with a higher flame temperature and speed near the centreline. However, flame acceleration can potentially be weaker at the centreline, with the promotion at the wall, say, as is often observed in coalmines. In that case, combustible coal dust particles may be present, being distributed along a tunnel wall, which can promote flame acceleration nearby the wall region (at least for certain ranges of the sizes and concentrations of the dust particles). In order to consider promotion of flame propagation along the wall and its moderation at the centreline, a parabolic function of Equation (1) can be modified as:

$$S_L^* = S_{L,0}\left(0.2 + \varsigma\left(\frac{x}{R}\right)^2\right). \tag{13}$$

In particular, in the present work we employ $\varsigma = 0.8$. In that case, the flame exhibits the earlier defined reference speed $S_{L,0}$ at the wall and $0.2\,S_{L,0}$ at the centreline, which is exactly opposite to Equation (1). Again, it is noted that a and ς are free parameters of the

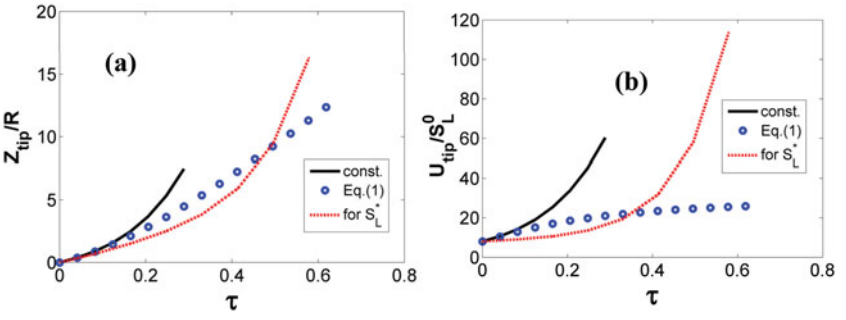

Figure 7. 2D planar geometry: evolution of the scaled flame tip position (a) and velocity (b).

problem, chosen arbitrarily. The parabolic and constant S_L-distributions in that case are compared in Figure 7 for Z_{tip} (Figure 7(a)) and U_{tip} (Figure 7(b)). Based on Figure 7, we can arrive to the following physical interpretation: when Equation (1) is employed, yielding promotion of flame propagation through the centreline and its moderation through the walls, the larger flame surface area is observed through the wall segments, but the local flame speed is lower through the upper and lower sidewalls. On the other hand, Equation (13) is used again, promoting the flame spreading at the wall and moderating flame propagation at the centreline. While the larger surface area is observed at the wall region, this time, the local flame speed is however higher at the wall regions as well. Since the burning rate increases with the flame surface area, the highest flame tip velocity is obtained for S_L^* of Equation (13), even the same (parabolic) type is employed with the same magnitudes but locally opposite.

4. Validation by the computational simulations

To validate the theory, we next perform computational simulations of the combustion equations in a 2D planar geometry. The core of the computational platform was originally developed at Volvo Aero, Gotheborg, Sweden,, and constituted of a Navier–Stokes code solving for the reacting flow equations with fully compressible hydrodynamics, transport properties (heat conduction, diffusion and viscosity) and one-step Arrhenius chemical kinetics. This solver is based on a cell-centred, finite-volume scheme, which is of the 2nd-order accuracy in time and the 4th-order accuracy in space for the convective terms, and the 2nd-order accurate in space for the diffusive terms. The platform is adapted to parallel computations and it has been successfully validated on numerous complex combustion and aero-acoustic problems [2,19,23]. More details about the computational platform can be found, in particular, in [19]. The governing equations in a 2D planar geometry read:

$$\frac{\partial}{\partial t}\rho + \frac{\partial}{\partial x_i}(\rho u_i) = 0, \tag{14}$$

$$\frac{\partial}{\partial t}(\rho u_i) + \frac{\partial}{\partial x_j}\left(\rho u_i u_j + \delta_{i,j}P\right) - \gamma_{i,j} = 0, \tag{15}$$

$$\frac{\partial}{\partial t}\left(\rho\varepsilon + \frac{1}{2}\rho u_i u_j\right) + \frac{\partial}{\partial x_i}\left(\rho u_i h + \frac{1}{2}\rho u_i u_j u_j + q_i - u_j\gamma_{i,j}\right) = 0, \tag{16}$$

$$\frac{\partial}{\partial t}(\rho Y) + \frac{\partial}{\partial x_i}\left(\rho u_i Y - \frac{\zeta}{\mathrm{Sc}}\frac{\partial Y}{\partial x_i}\right) = -\frac{\rho Y}{\tau_R}\exp\left(-E_a/R_u T\right), \tag{17}$$

where the progress variable Y describes the mass fraction of the fuel mixture, $\varepsilon = QY + C_vT$ is the specific internal energy, $h = QY + C_pT$ the specific enthalpy, $Q = C_pT_f(\Theta - 1)$ the energy release in the reaction, Θ the thermal expansion ratio, and C_v, C_P the specific heats at constant volume and pressure, respectively. Equation (17) describes a single irreversible Arrhenius reaction of the first order, with the activation energy E_a and the constant of time dimension τ_R. The stress tensor $\gamma_{i,j}$ and the energy diffusion vector q_i are given by:

$$\gamma_{i,j} = \zeta\left(\frac{\partial u_i}{\partial x} + \frac{\partial u_j}{\partial x_i} - \frac{2}{3}\frac{\partial u_k}{\partial x_k}\delta_{i,j}\right), \qquad q_i = -\zeta\left(\frac{C_p}{\mathrm{Pr}}\frac{\partial T}{\partial x_i} + \frac{Q}{\mathrm{Sc}}\frac{\partial Y}{\partial x_i}\right), \tag{18}$$

where $\zeta \equiv \rho\nu$ is the dynamic viscosity, with Pr and Sc being the Prandtl and Schmidt numbers, respectively. The burnt and unburned gases are assumed to be ideal gases of identical molecular weights W_M and thereby the equation of state is $P = \rho R_u T/W_M$, with the universal gas constant $R_u = 8.31$ kJ (kmol K)$^{-1}$.

In all the simulations, a flame was initiated by means of the Zeldovich–Frank–Kamenetsky (ZFK) analytical solution [24] for an initially hemispheric flame embryo propagating in a semi-open channel with adiabatic and slip walls, from a closed end to an open extreme. Additionally, to avoid any potential impact of the weak shocks and sound waves reflected from the ends, the non-reflecting boundary conditions are employed at the open extreme of the channel [19].

Since we aim to resolve the flame structure, an appropriate grid size is determined by the flame thickness. The latter is conventionally defined as the thermal diffusivity to the planar flame speed ratio, $L_f \equiv D_{th}/S_L$ [2] (it is nevertheless noted that L_f is a characteristic length scale, while a realistic flame zone can be up to an order of magnitude wider [4]). An appropriate resolution also depends on the choice of the activation energy E_a. Similar to [19], here we employ a quite moderate activation energy, $E_a/RT_b = 4$, in order to spread the active reaction zone over several computational cells. The unstretched laminar flame velocity S_L depends on the three major chemical parameters of the fuel mixture, namely: Q, E_a and τ_R. While in our previous numerical studies [2,19,23] the value S_L was constant over the entire computational domain such that the values Q, E_a and τ_R were fixed too, in the present work S_L is a spatial function. To be specific, we obtained S_L-variations in space by varying τ_R at fixed Q and E_a.

The computational simulations for a constant, linear, parabolic and hyperbolic distribution of S_L, Equation (1), are compared in Figure 8, where the scaled flame tip velocity U_{tip}/S_L is plotted versus the scaled time τ for all these cases. Similar to the theoretical predictions of Sections 2–3, the simulations also show that all the S_L-variations considered here moderate flame acceleration as compared to the case of a constant S_L. Indeed, the curve for a hyperbolic S_L-distribution goes lower than that for S_L= *const.*, followed by the curves for the parabolic and linear distributions of S_L, respectively. It is also seen that the difference between the parabolic and hyperbolic cases is minor, whereas both these curves differ from the curves for linear and constant S_L.

We next compare the theoretical predictions with the computational results in Figures 9–12. Specifically, Figure 9 is devoted to a constant S_L, whereas a linear distribution of S_L is described in Figure 10, a parabolic distribution is in Figure 11, and Figure 12 shows a hyperbolic S_L-distribution. In all these cases, the (a) subfigures compare the evolutions of the scaled instantaneous flame tip positions, Z_{tip}/R, while the evolutions of the scaled instantaneous velocities of the flame tip, in the laboratory reference frame, $U_{tip}/S_{L,0}$, are compared in the (b) parts of Figures 9–12.

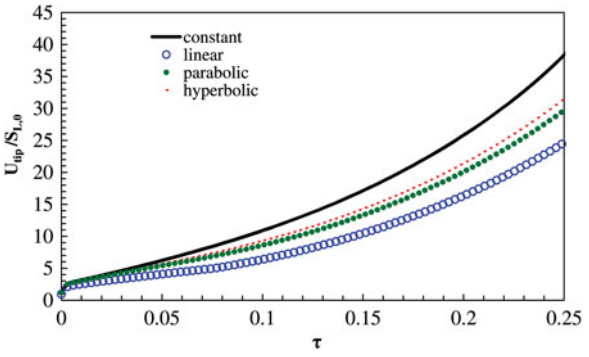

Figure 8. Computational simulations: evolution of the scaled flame tip velocity for the constant, linear, parabolic and hyperbolic S_L-distributions.

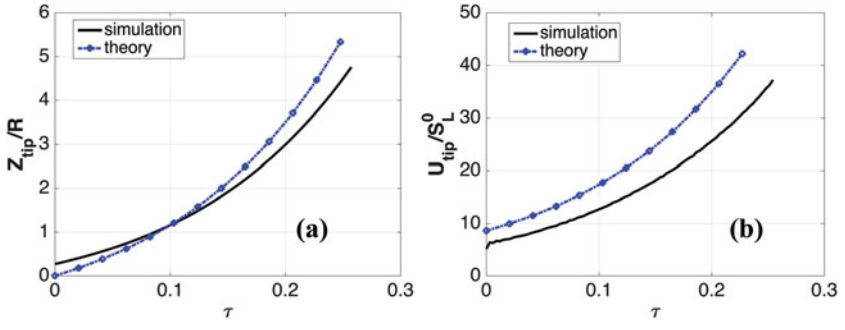

Figure 9. Comparison of the computational simulations and the theoretical predictions for a constant S_L: evolution of the scaled flame tip position (a) and velocity (b).

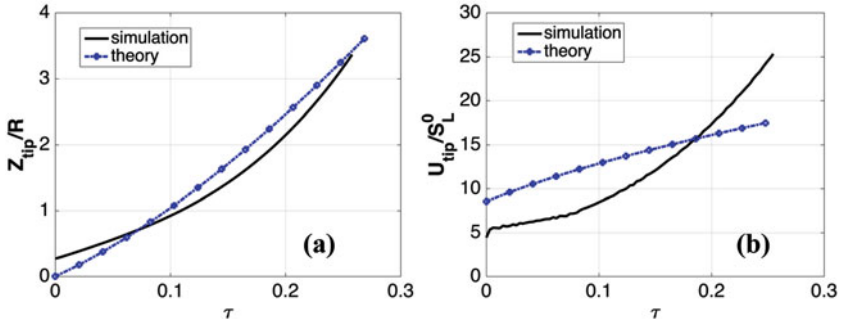

Figure 10. Comparison of the computational simulations and the theoretical predictions for a linear S_L-distribution: evolution of the scaled flame tip position (a) and velocity (b).

Overall, agreement between the theory and modelling is observed in all Figures 9–12, thereby justifying the theoretical formulation of the present work. Specifically, this agreement is good in Figures 9(a)–12(a), for the flame tip position, and it is reasonable in Figures 9(b)–12(b), for the flame tip velocity, especially at the initial stage of the burning process.

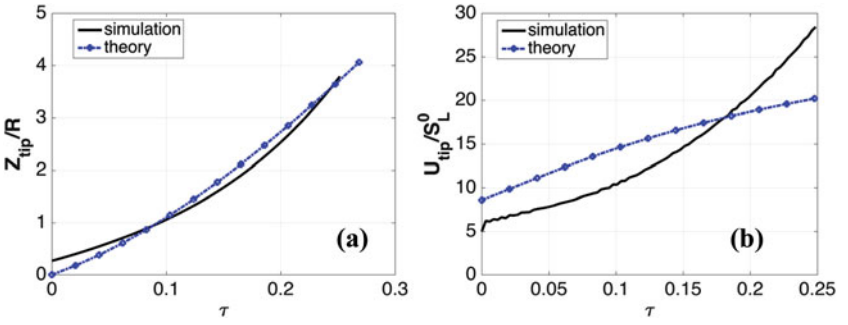

Figure 11. Comparison of the computational simulations and the theoretical predictions for a parabolic S_L-distribution: evolution of the scaled flame tip position (a) and velocity (b).

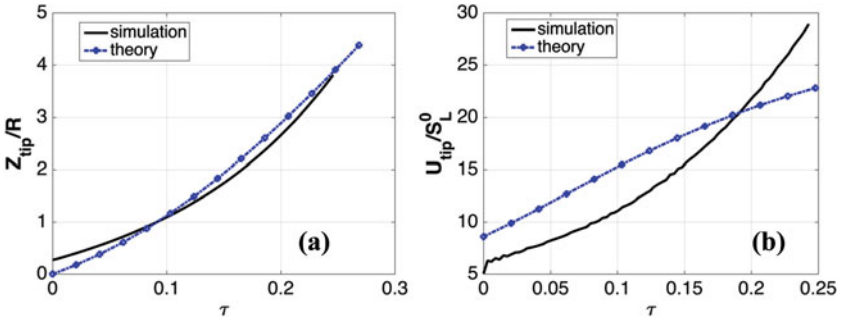

Figure 12. Comparison of the computational simulations and the theoretical predictions for a hyperbolic S_L-distribution: evolution of the scaled flame tip position (a) and velocity (b).

5. Discussion and summary

In this study, various spatial distributions (constant, linear, parabolic and hyperbolic) of the planar flame velocity S_L are incorporated into a theory of flame acceleration due to a finger-like flame shape [5]. Revisited equations for the flame skirt, Equations (6) and (11), and the flame tip, Equations (11) and (12), are obtained for the 2D planar and cylindrical axisymmetric cases, respectively. These results are presented in Figures 4 and 5, and they are compared in Figure 6. It is demonstrated, qualitatively and quantitatively, that the geometry influences the flame acceleration mechanism. Specifically, in the cylindrical axisymmetric geometry, a flame accelerates faster as compared to the 2D planar case for all distributions considered, including the case of $S_L = S_{L,0} = const$. It is pointed out that the concept of spatial variation of the laminar flame speed S_L can moderate or promote a global flame acceleration mechanism. Indeed, different imposed S_L-functions may provide different controlling strategies to mitigate flame acceleration. As a result, imposing various S_L-distributions can potentially be a useful tool to control a flame acceleration scenario.

The theoretical analysis is supported by the ad-hoc computational simulations. Agreement between the theory and modelling, demonstrated in Figures 9–12, thereby validates the formulation. The practical applications of this work include, in particular, methane–air fire safety issues in coalmines with dusty atmosphere. It is recalled again that the coal dust distribution is typically non-uniform in coalmines, where a stationary dense coal dust layer may spread through the bottom of a passage. In particular, a gaseous-based detonation wave may produce a strong shock that can lift and entrain the dust layer. Over time, this shock

wave weakens, but the fluid, heated by the shock wave, is ignited by the lifted dust, which initiates a secondary combustion process [22]. Such a lifted dust layer may resemble a linear, a cubic, or even a parabolic distribution of the dust concentration in space, due to the different energy levels of complex magnetic forces. To account for the combustible and/or inert dust particles in a global flame-spreading scenario, for instance, the Seshadri formulation [11] can be employed, according to which the planar flame velocity in a dusty–gaseous mixture $S_{L,d}$ can be expressed as a function of a number of the dusty parameters including the size and the concentration of the dust particles. Then, to model the spatial variation of the flame velocity, various non-uniform dust distribution gradients can be employed into the analysis.

Finally, it is recalled that the present work initiates a systematic study of how to incorporate the local variations of the planar flame velocity into a formulation on the global, corrugated flame velocity. In this respect, the present study is only the first step in this direction, with only four S_L-distributions used, while it is recognised that other distributions might also be employed.

Acknowledgements

This study was sponsored by the US National Science Foundation (NSF) through the CAREER Award #1554254 (V.A.) as well as by the West Virginia Higher Education Policy Commission through the grant #HEPC.dsr.18.7 (V.A.).

Funding

This work was supported by the US National Science Foundation (NSF) [grant number CAREER Award #1554254]; and West Virginia Higher Education Policy Commission [grant number #HEPC.dsr.18.7]

Disclosure statement

No potential conflict of interest was reported by the authors.

References

[1] C.K. Law, *Combustion Physics*, Cambridge University Press, New York, 2006.
[2] V. Bychkov, A. Petchenko, V. Akkerman, and L.-E. Eriksson, *Theory and modeling of accelerating flames in tubes*, Phys. Rev. E 72 (2005), p. 046307.
[3] K.I. Shelkin, *Influence of tube non-uniformities on the detonation ignition and propagation in gases*, Zh. Eksp.Teor. Fiz. 10 (1940), pp. 823–827.
[4] V. Akkerman, V. Bychkov, A. Petchenko, and L.-E. Eriksson, *Accelerating flames in cylindrical tubes with nonslip at the walls*, Combust. Flame 145 (2006), pp. 206–219.
[5] V. Bychkov, V. Akkerman, G. Fru, A. Petchenko, and L.-E. Eriksson, *Flame acceleration in the early stages of burning in tubes*, Combust. Flame 150 (2007), pp. 263–276.
[6] V. Akkerman, C.K. Law, V. Bychkov, and L.-E. Eriksson, *Analysis of flame acceleration induced by wall friction in open tubes*, Phys. Fluids 22 (2010), p. 053606.
[7] V.N. Kurdyumov and C. Jiménez, *Propagation of symmetric and non-symmetric premixed flames in narrow channels: Influence of conductive heat-losses*, Combust. Flame 161 (2014), pp. 927–936.
[8] C.E. Frouzakis, N. Fogla, A.G. Tomboulides, C. Altantzis, and M. Matalon, *Numerical study of unstable hydrogen/air flames: Shape and propagation speed*, Proc. Combust. Inst. 35 (2015), pp. 1087–1095.
[9] M. Metghalchi and J.C. Keck, *Burning velocities of mixtures of air with methanol, isooctane, and indolene at high pressure and temperature*, Combust. Flame 48 (1982), pp. 191–210.

[10] R. Sankaran, H.G. Im, E.R. Hawkes, and J.H. Chen, *The effects of non-uniform temperature distribution on the ignition of a lean homogeneous hydrogen–air mixture*, Proc. Combust. Inst. 30 (2005), pp. 875–882.
[11] K. Seshadri, A.L. Berlad, and V. Tangirala, *The structure of premixed particle-cloud flames*, Combust. Flame 89 (1992), pp. 333–342.
[12] S.R. Rockwell and A.S. Rangwala, *Modeling of dust air flames*, Fire Safety J. 59 (2013), pp. 22–29.
[13] J. Grune, K. Sempert, H. Haberstroh, M. Kuznetsov, and T. Jordan, *Experimental investigation of hydrogene -air deflagrations and detonations in semi-confined flat layers*, J. Loss Prevent. Process Ind. 26 (2013), pp. 317–323.
[14] J. Grune, K. Sempert, M. Kuznetsov, and T. Jordan, *Experimental investigation of fast flame propagation in stratified hydrogeneair mixtures in semi-confined flat layers*, J. Loss Prevent. Process Ind. 26 (2013), pp. 1442–1451.
[15] X. Shi, J.Y. Chen, and Z. Chen, *Numerical study of laminar flame speed of fuel-stratified hydrogen/air flames*, Combust. Flame 163 (2016), pp. 394–405.
[16] S. Hemchandra and T. Lieuwen, *Local consumption speed of turbulent premixed flames – An analysis of "memory effects*, Combust. Flame 157 (2010), pp. 955–965.
[17] D. Valiev, V. Bychkov, V. Akkerman, C.K. Law, and L.-E. Eriksson, *Flame acceleration in channels with obstacles in the deflagration-to-detonation transition*, Combust. Flame 157 (2010), pp. 1012–1021.
[18] C. Clanet and G. Searby, *On the "tulip flame" phenomenon*, Combust. Flame 105 (1996), pp. 225–238.
[19] D. Valiev, V. Akkerman, M. Kuznetsov, L.-E. Eriksson, C.K. Law, and V. Bychkov, *Influence of gas compression on flame acceleration in the early stage of burning in tubes*, Combust. Flame 160 (2013), pp. 97–111.
[20] S. Demir, V. Bychkov, S.H.R. Chalagalla, and V. Akkerman, *Towards a predictive scenario of a burning accident in a mining passage*, Combust. Theory Model. 21 (2017), pp. 997–1022.
[21] S. Demir, A.R. Calavay, and V. Akkerman, *Influence of gas compressibility on a burning accident in a mining*, Combust. Theory Model. 22 (2018), pp. 338–358.
[22] R.W. Houim and E.S. Oran, *Numerical simulation of dilute and dense layered coal-dust explosions*, Proc. Combust. Inst. 35 (2015), pp. 2083–2090.
[23] A. Petchenko, V. Bychkov, V. Akkerman, and L.-E. Eriksson, *Violent folding of a flame front in a flame-acoustic resonance*, Phys. Rev. Lett. 97 (2006), p. 164501.
[24] Y.B. Zeldovich and D. Frank-Kamenetski, *A theory of thermal propagation of flames*, Acta Physicochim URSS 12 (1938), pp. 341–350.